Journal of Zhejiang University-SCIENCE A (Applied Physics & Engineering) *2025 26(4):305-319*
www.jzus.zju.edu.cn; www.springer.com/journal/11582
E-mail: jzus_a@zju.edu.cn

Research Article
https://doi.org/10.1631/jzus.A2400521

Thermodynamics-based simulations of the hydration of low-heat Portland cement and the compensatory effect of magnesium oxide admixtures

Wenwei LI[1,2], Yifan ZHOU[3], Jiajie YIN[3], Yuxiang PENG[3], Yushan WANG[4], Shengwen TANG[3,5]✉, Yan SHI[2], Yang WANG[3], Lei WANG[6]

[1]*China Three Gorges Corporation, Beijing 100038, China*
[2]*Changjiang River Scientific Research Institute of Changjiang Water Resources Commission, Wuhan 430010, China*
[3]*State Key Laboratory of Water Resources Engineering and Management, Wuhan University, Wuhan 430072, China*
[4]*School of Urban Construction, Wuhan University of Science and Technology, Wuhan 430065, China*
[5]*Henan Key Laboratory of Green Building Materials Manufacturing and Intelligent Equipment, Luoyang Institute of Science and Technology, Luoyang 471023, China*
[6]*College of Materials Science and Engineering, Xi' an University of Architecture and Technology, Xi' an 710055, China*

Abstract: Low-heat Portland (LHP) cement is a new type of Portland cement that has been widely used in recent years due to its low heat of hydration, which makes it exceptional in temperature control for mass concrete construction. However, limited studies have investigated the impact of temperature and magnesium oxide (MgO) content on LHP cement-based materials. This study utilizes thermodynamic simulations to study the hydration process, pore structure, and autogenous shrinkage of LHP cement pastes with different water-to-cement ratios (0.3, 0.4, and 0.5), curing temperatures (5, 15, 20, and 30 °C), and MgO contents (mass fractions of 2%, 4%, and 5%). Higher curing temperature is found to promote the hydration reactions in cement paste. Moreover, the incorporation of 4% MgO moderately decreases both porosity and dimensional shrinkage in pastes. The microstructural evolution of different LHP pastes is examined through a comparative analysis, lending insights into LHP cement-based material applications.

Key words: Low-heat Portland cement (LHP); Shrinkage; Magnesium oxide expansion; Thermodynamic modeling; Hydration; Pore structure

1 Introduction

Concrete is one of the most prevalent materials around the world and plays a vital role in the development of infrastructure. Scientific study of concrete materials is imperative for advancing civil engineering technology. After over a century of research, our understanding of concrete materials has grown massively (van Damme, 2018). However, to meet the high-performance demands of modern engineering projects, there is significant need for further development in concrete materials. Low-heat Portland (LHP) cement, also known as high-belite Portland cement, offers advantages such as low heat of hydration, low energy consumption, low CO_2 emissions, excellent crack resistance, good workability, and others (Yang et al., 2007; Xie et al., 2023). In recent years, LHP cement has been widely used in large-scale concrete projects. A notable example is the Wudongde Dam in China, where LHP cement is used throughout the structure. LHP cement has proved to be effective in mitigating cracking associated with mass concrete during dam construction (Peng et al., 2022).

The principal difference between LHP cement and ordinary Portland cement is their mineralogical compositions. Specifically, LHP cement contains a large amount of C_2S and little C_3S. Since the heat of hydration released by C_3S is larger and its exothermic peak occurs earlier than in C_2S, reducing C_3S and

✉ Shengwen TANG, tangsw@whu.edu.cn
Shengwen TANG, https://orcid.org/0000-0002-4883-3103

Received Nov. 10, 2024; Revision accepted Jan. 7, 2025;
Crosschecked Apr. 6, 2025

increasing C_2S content enables significant reduction in the heat of hydration while still maintaining late strength (Sinyoung et al., 2017; Gong et al., 2020). However, the lower degree of hydration of C_2S compared to C_3S in Portland cement can affect the early hydration of LHP cement-based materials, potentially resulting in reduced early compressive strength (Kotsay and Jaskulski, 2019; Gong et al., 2020; Cuesta et al., 2021; Wang et al., 2022).

Additionally, most of the remaining hydropower resources in China are distributed in the West and Southwest. Because of the large temperature differences at these locations, it is important to investigate the microstructural evolution of LHP cement-based materials at different curing temperatures (Vahedifard et al., 2010).

Temperature-induced thermal stresses in cement paste can lead to shrinkage (Yang et al., 2024). The phenomenon of chemical shrinkage can also arise due to the volumetric changes from chemical hydration (Bentz and Jensen, 2004). Shrinkage is a significant factor impacting crack formation in concrete. As previously noted, the primary advantage of LHP cement is its low heat of hydration (Xie et al., 2023), which endows it with resistance to shrinkage. However, to accommodate large-scale concrete structures, it is sometimes necessary to introduce admixtures to the concrete to achieve better crack resistance. Sourced from calcined magnesite or magnesium-rich minerals, MgO has been extensively implemented in some dam projects since 1980s, demonstrating high efficacy in the thermal crack mitigation through expansive compensation (Chen et al., 2016). MgO can effectively compensate for part of the autogenous shrinkage due to its expansive effect, which can lower the cracking risk (Mo et al., 2014). The amount and reactivity of MgO in the concrete significantly affects the shrinkage compensation effectiveness.

In a previous study, changes in the ion concentration of the pore solution of Portland cement paste and various substances in the phase dissolution and precipitation process were simulated by establishing a Portland cement thermodynamic database; this was done after evaluating the thermodynamic data of the Portland mineral phase (Brouwers and de Korte, 2016).

Investigations of the hydration characteristics in LHP cementitious materials have predominantly depended on experimental approaches, and a modeling approach could reveal new insights. In addition, LHP cement-based materials are widely used in hydraulic projects. However, the influence of MgO and water-to-cement ratio on the LHP cement-based materials is still not clear from the view point of computer modeling. Therefore, further investigation of the hydration mechanism in LHP cement-based materials is needed. In this study, by utilizing computer simulations, we investigate the hydration and autogenous shrinkage of LHP cement paste with varying water-to-cement ratios and different curing temperatures, as well as the impact of MgO content on the shrinkage of LHP cement pastes.

2 Methods and algorithms

2.1 Hydration simulation method

This study investigates the impacts of curing temperature, water-to-cement ratio, and MgO content on the hydration products and shrinkage of LHP cement paste. Notations for the different pastes and their mixing proportions are shown in Table 1. The chemical and mineral compositions of LHP raw clinkers are shown in Table 2.

Table 1 Paste notations and mixing proportions of LHP cement pastes

Notation	Water-to-cement ratio	Temperature (°C)	Mass fraction of MgO (%)
WC04T5M0	0.40	5	0
WC04T15M0	0.40	15	0
WC04T20M0	0.40	20	0
WC04T30M0	0.40	30	0
WC045T5M0	0.45	5	0
WC045T15M0	0.45	15	0
WC045T20M0	0.45	20	0
WC045T30M0	0.45	30	0
WC05T5M0	0.50	5	0
WC05T15M0	0.50	15	0
WC05T20M0	0.50	20	0
WC05T30M0	0.50	30	0
WC04T20M2	0.40	20	2
WC04T20M4	0.40	20	4
WC04T20M5	0.40	20	5
WC045T20M2	0.45	20	2
WC045T20M4	0.45	20	4
WC045T20M5	0.45	20	5
WC05T20M2	0.50	20	2
WC05T20M4	0.50	20	4
WC05T20M5	0.50	20	5

Table 2 Chemical and mineral compositions of LHP raw clinkers

Chemical composition	Mass fraction (%)	Mineral composition	Mass fraction (%)
CaO	61.86	C_3S	28.7[b] (30.7)[c]
SiO_2	23.98	C_2S	47.0[b] (44.3)[c]
Fe_2O_3	4.22	C_3A	4.1[b] (3.6)[c]
Al_2O_3	4.23	C_4AF	12.8[b] (14.1)[c]
MgO	2.89	Gypsum	3.9
SO_3	2.31		
R_2O [a]	0.31		
Loss on ignition (%)	0.45		

[a] Alkali content (mass fraction): $R_2O=Na_2O+0.658K_2O$; [b] From Bogue analysis; [c] From X-ray analysis (Zhou et al., 2023)

GEM-Selektor (GEMS) is a computational suite specialized for Gibbs free energy minimization, extensively applied for simulating multiphase geochemical aqueous systems. It focuses on interactive thermodynamics, including solid-aqueous solution equilibria, sorption/ion exchange processes, and the metastability and dispersion of mineral phases (Karpov et al., 1997, 2001; Wagner et al., 2012; Kulik et al., 2013). Initially, relevant thermodynamic data suitable for LHP cement should be selected; in this study, the CEMDATA18 database was used (Lothenbach et al., 2019). Subsequently, the hydration data of LHP cement, including standard Gibbs free energy, entropy, and volume were utilized. The equilibrium hydration products of cement pastes under different conditions were computed. The input parameters of the simulation also included the curing temperature, water-to-cement ratio, and MgO content. Based on the GEMS thermodynamic simulation results, the initial and in-process stages of hydration products in the LHP cement paste were visualized using MATLAB to evaluate the effect of input parameters.

2.2 Determination of pore structure

The mechanical properties and durability of cement-based materials are mainly determined by their pore structure (Zhong et al., 2022a, 2022b, 2023a, 2023b, 2024). In this study, the disk filling method algorithm was employed to calculate the porosity of LHP cement paste at specific stages (Song et al., 2019). In this algorithm, the pores are assumed to be filled by disks. The size of the disks increased as the reaction progressed once all the pores were filled. As a result, the overall porosity of LHP cement pastes could be determined.

2.3 MgO expansion simulation method

Based on the visualization obtained from MATLAB, a 100 μm×100 μm×100 μm cube and a resolution of 0.1 μm were adopted in this work (Zhang et al., 2010; Ma and Li, 2013). To investigate the impact of MgO content on the microstructural evolution of LHP cement paste, an autogenous shrinkage model for the cement paste was developed. The shrinkage was assumed to be primarily induced by volumetric changes in the hydration products. Autogenous shrinkage refers to the overall deformation of cement-based materials in a closed, isothermal system. It is mainly caused by autogenous drying, which is a result of volume shrinkage during cement hydration. This shrinkage is related to the surface tension between liquid and gas phases in capillary pores (Zhang, 2022).

The autogenous shrinkage model consisted of three main parts: the input module, the autogenous drying module, and the capillary pressure and shrinkage deformation modules. In the input module, the 3D microstructure was incorporated. Hydration products and relative humidity of the cement paste were simulated using GEMS and thermodynamic models. In the autogenous drying module, the distributions of moisture and empty capillary pores within the cement paste were considered. In the capillary pressure and shrinkage deformation modules, the capillary pressure within the cement paste was calculated using the Kelvin equation and the Young-Laplace equation. Capillary pressure was assumed to uniformly distribute across a 3D grid of the pastes. A finite element method was used to simulate the deformation of the cement paste due to autogenous drying, and a discrete algorithm integrated the deformations over time to yield the self-induced shrin-kage of the cement paste (Jawed et al., 1976; Hilpert and Miller, 2001; Qian et al., 2010).

3 Results and discussion

3.1 Effect of temperature on hydration of LHP paste

In this work, distinct colors were used to represent particles and phases of the cement paste, as shown in Table 3. To facilitate the analysis, cross-sectional

Table 3 Distinct colors for particles and phases of the cement paste

Particle	Color	Phase	Color
C_3S	Red	Pore or water	Dark blue
C_2S	Pink	Crystals and gel[a]	Purple
C_3A	Orange	MH crystals[b]	Cyan
C_4AF	Deep yellow	Outer hydration product	Green
Other non-hydrated raw clinker	Grey	Inner hydration product	Light yellow
MgO	Black		

[a] Crystals and gel include C–S–H, CH, AFt, AFm, and hydrotalcite; [b] MH crystals are from the hydration of MgO particles (Zhou et al., 2023)

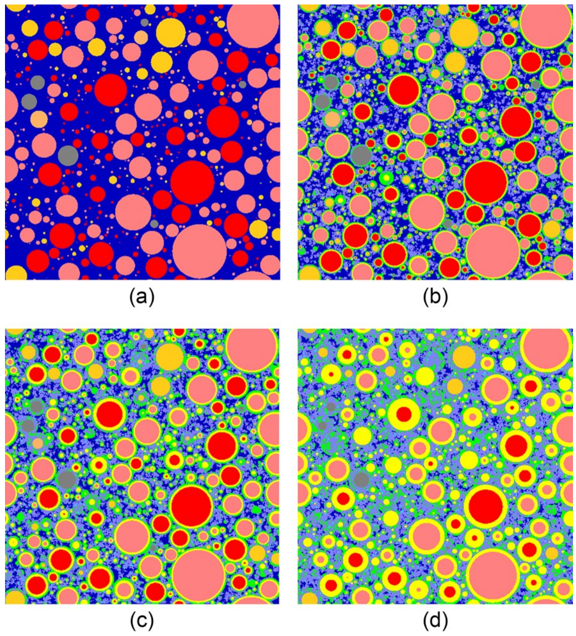

Fig. 1 Cross-sectional diagram of Paste WC04T5M0: (a) initial state; (b) curing for 1 d; (c) curing for 3 d; (d) curing for 27 d

diagrams of different simulated pastes were collected for comparative examination. Fig. 1 is a cross-section of Paste WC04T5M0. References to color refer to the online version of Figs. 1–21. Fig. 1a represents the initial state of Paste WC04T5M0, where the scattered spheres represent different cement particles within the paste; Fig. 1b shows the hydration state of Paste WC04T5M0 when the curing time is 1 d, which reveals that particles within the paste have commenced hydration reactions, with yellow internal hydration products closely enveloping the particles. Some green external hydration products are observed, which exhibit a dispersed structure compared to the internal products. Notably, certain areas intertwine with purple phases, which are distributed broadly throughout the paste, facilitating potential connections between the previously isolated cement particles.

In Fig. 1c, it can be observed that at a curing duration of 3 d, there is a significant increase in the content of purple phases within the paste, indicating the formation of a relatively loose skeletal structure. Internal hydration processes continue, leading to a noticeable thickening of the layer of hydration products surrounding the cement particles. In contrast, if we observe Fig. 1d, after 27 d of curing, a substantial quantity of hydrated products has filled the original voids, resulting in a dense microstructure in the paste. It is evident that some of the small particles hydrate quickly, whereas large particles may keep non-hydrated regions in their cores. This may be attributed to the development of a compact layer of internal hydration products over the prolonged hydration period, which hinders water penetration into the interior of cement particles and the subsequent precipitation of internal hydrated products (Bullard et al., 2011).

To investigate the influence of curing temperature on the hydration of LHP cement pastes, corresponding simulations were performed as illustrated in Figs. 2–4. A comparative analysis of Figs. 1–4 reveals that, for equivalent hydration durations, high temperatures correlate with an increased quantity of hydration products and greater reactivity of the cement particles within the investigated temperature range. In summary, it can be concluded that high curing temperatures facilitate the cement hydration reaction. Specifically, at a curing temperature of 30 °C, the overall microstructure of the paste is denser compared to that at 5 °C for the same hydration time. Notably, for hydration times of 1 and 3 d, Figs. 1b and 1c distinctly illustrate the temperature-induced differences, showing that high temperatures yield larger quantities of hydration products and a denser paste structure. However, when curing for 27 d, a comparison of Figs. 1d–4d indicates that the structural differences are not as pronounced. This suggests that, at 27 d, temperature may no longer be a primary factor affecting the continued hydration of cement.

Previous work also confirmed that high curing temperature might eliminate ion diffusion by forming

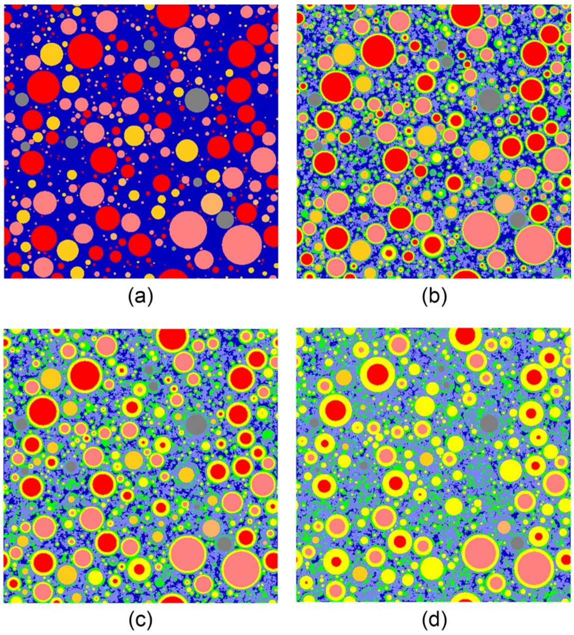

Fig. 2 Cross-sectional diagram of Paste WC04T15M0: (a) initial state; (b) curing for 1 d; (c) curing for 3 d; (d) curing for 27 d

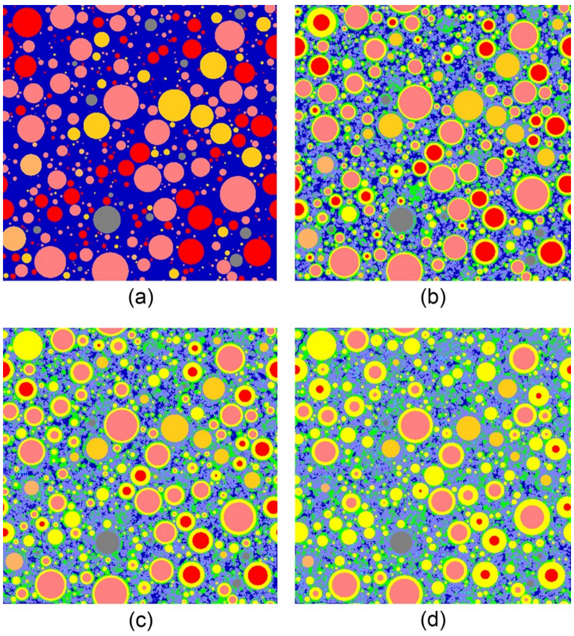

Fig. 3 Cross-sectional diagram of Paste WC04T20M0: (a) initial state; (b) curing for 1 d; (c) curing for 3 d; (d) curing for 27 d

a thick covering layer upon the non-hydrated particles, and thus, reduce the long-term strength of the cement paste (Yi et al., 2005). Other studies also pointed out that this covering layer exerts a delaying effect on the precipitation of hydrated products (Kjellsen and Detwiler,

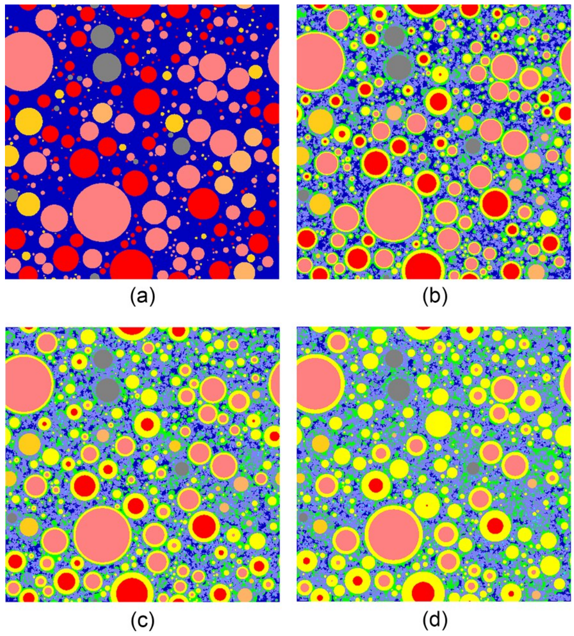

Fig. 4 Cross-sectional diagram of Paste WC04T30M0: (a) initial state; (b) curing for 1 d; (c) curing for 3 d; (d) curing for 27 d

1992, 1993; Fang and Fall, 2018). The phenomena observed in this simulation aligns with the findings of previous studies, indicating that rapid early hydration under high temperature curing indeed leads to the formation of a relatively dense layer of hydration products surrounding the cement particles. This layer hinders the further precipitation of hydration products and the continued hydration of particles, resulting in a diminished influence of temperature on the hydration process during prolonged hydration periods.

3.2 Effect of water-to-cement ratio on hydration of LHP paste

To investigate the effect of the water-to-cement ratio on the hydration of LHP cement pastes, three water-to-cement ratios (0.40, 0.45, and 0.50) were tested. Cross-sectional diagrams of Pastes WC045T5M0, WC045T15M0, WC045T20M0, WC045T30M0, WC05T5M0, WC05T15M0, WC05T20M0, and WC05T30M0 with water-to-cement ratios of 0.45 and 0.50 are shown in Figs. 5–12. From a comparison of Figs. 1–12, it can be concluded that under the same hydration time and curing temperature, a high water-to-cement ratio usually results in more hydrated products in the paste. In other words, a high water-to-cement ratio corresponds to a high degree of cement particle

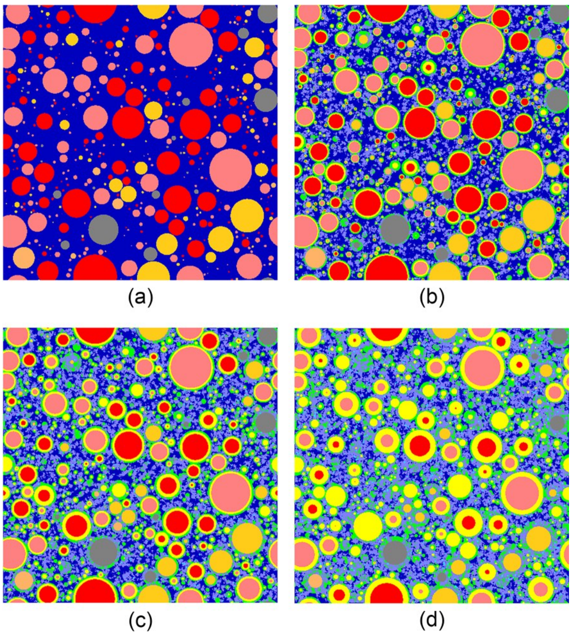

Fig. 5 Cross-sectional diagram of Paste WC045T5M0: (a) initial state; (b) curing for 1 d; (c) curing for 3 d; (d) curing for 27 d

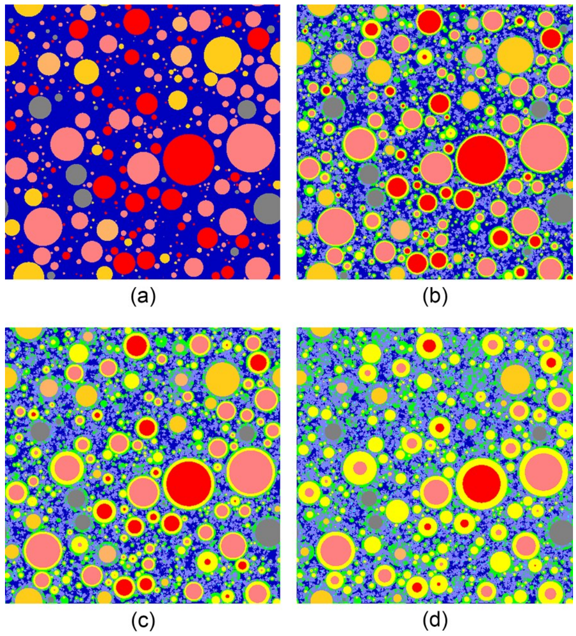

Fig. 7 Cross-sectional diagram of Paste WC045T20M0: (a) initial state; (b) curing for 1 d; (c) curing for 3 d; (d) curing for 27 d

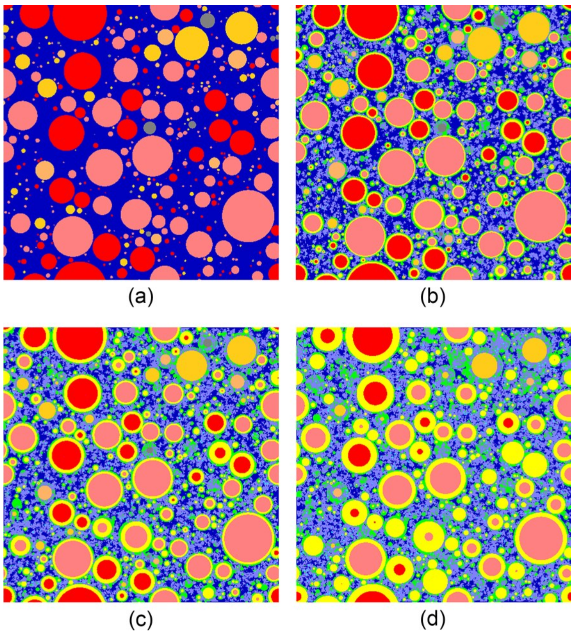

Fig. 6 Cross-sectional diagram of Paste WC045T15M0: (a) initial state; (b) curing for 1 d; (c) curing for 3 d; (d) curing for 27 d

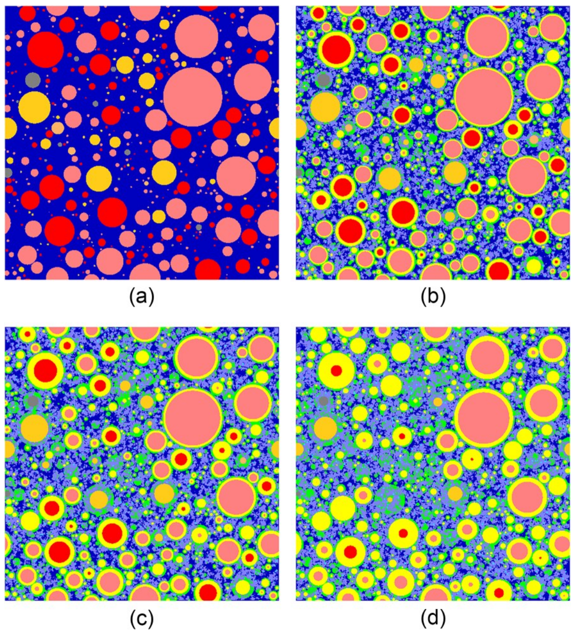

Fig. 8 Cross-sectional diagram of Paste WC045T30M0: (a) initial state; (b) curing for 1 d; (c) curing for 3 d; (d) curing for 27 d

hydration. For instance, as shown in Figs. 2d, 6d, and 9d, after 27 d of curing at 15 ℃, all cement pastes show a significant quantity of hydrated products and a relatively dense skeletal microstructure. However, due to the differences in water-to-cement ratios, the porosity of the pastes follows the trend WC04T15M0<WC045T15M0<WC05T15M0. Notably, for the pastes with a water-to-cement ratio of 0.50, the cement particles have thick internal and external hydrated product layers.

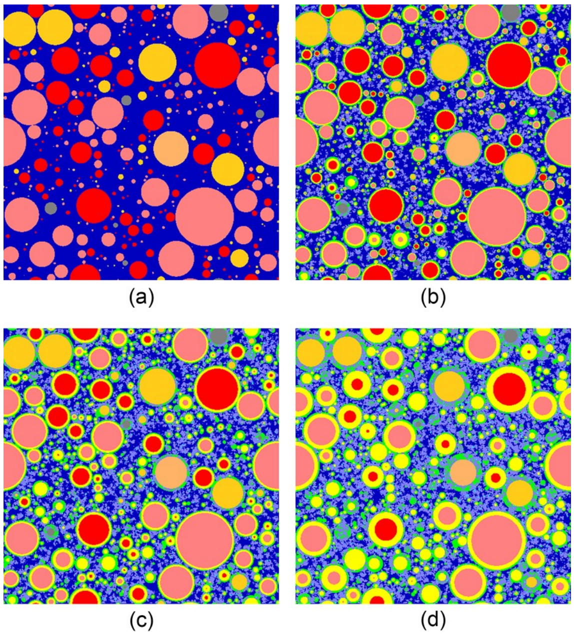

Fig. 9 Cross-sectional diagram of Paste WC05T5M0: (a) initial state; (b) curing for 1 d; (c) curing for 3 d; (d) curing for 27 d

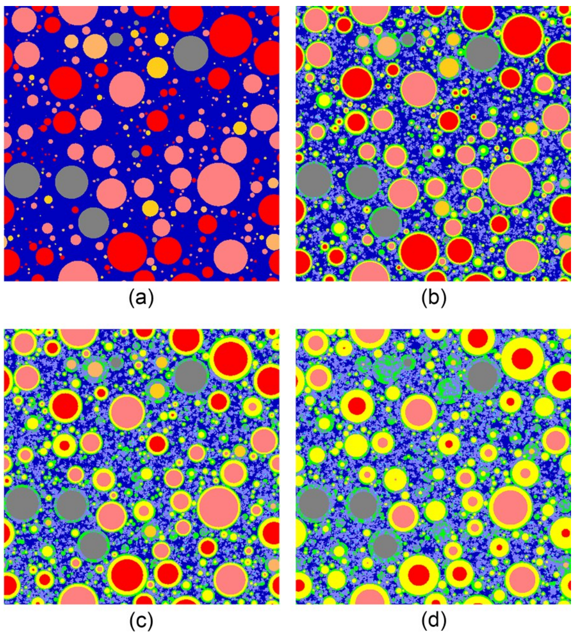

Fig. 10 Cross-sectional diagram of Paste WC05T15M0: (a) initial state; (b) curing for 1 d; (c) curing for 3 d; (d) curing for 27 d

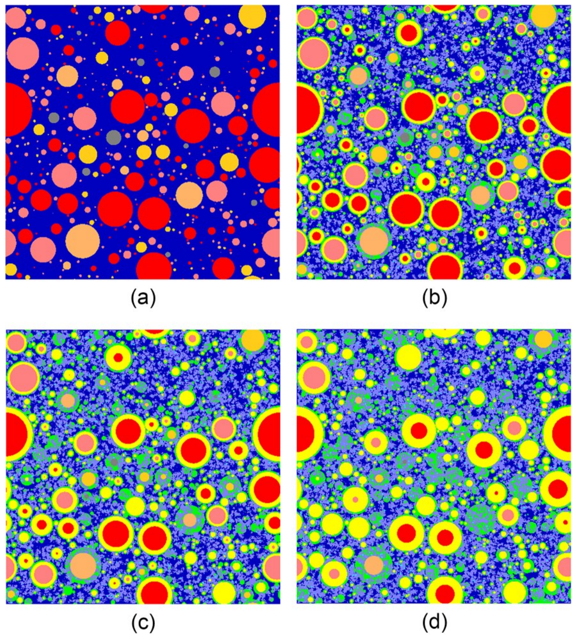

Fig. 11 Cross-sectional diagram of Paste WC05T20M0: (a) initial state; (b) curing for 1 d; (c) curing for 3 d; (d) curing for 27 d

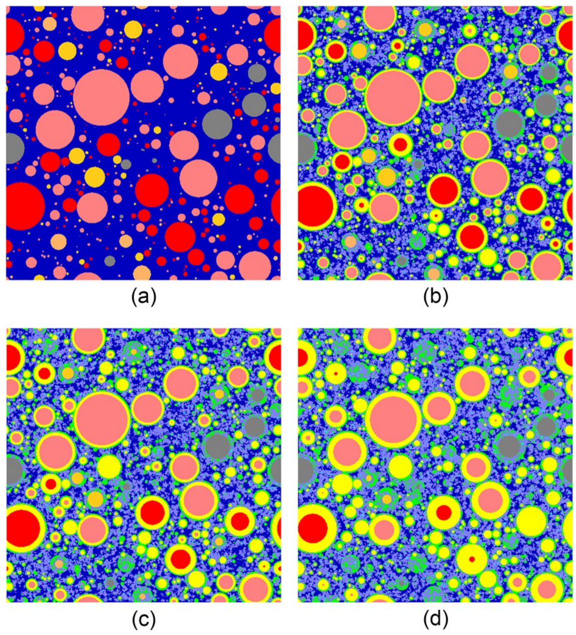

Fig. 12 Cross-sectional diagram of Paste WC05T30M0: (a) initial state; (b) curing for 1 d; (c) curing for 3 d; (d) curing for 27 d

Remarkably, while the overall quantity of hydrated products is low for the case of a high water-to-cement ratio, the cement particles can easily reach a high degree of hydration, resulting in efficient utilization of the particles. A similar trend is observed across the groups with different curing temperatures. Moreover, in pastes with low water-to-cement ratios, as the hydrated products gradually fill in the voids, the precipitation of hydrated products onto the cement particles becomes hindered. In contrast, pastes with high water-to-cement ratios offer more space for the cement particles to continue reacting. It is noteworthy those the low-heat cement used in this study contains a relatively high amount of C_2S, and under high water-to-cement ratios, the hydration rate of C_2S surpasses those of other raw clinker materials. After 14 d, the changes in hydrated product contents within the paste are likely driven primarily by C_2S hydration. This indicates that with sufficient hydration time, a high water-to-cement ratio not only enhances the hydration of raw clinker materials, but also promotes the hydration of C_2S (Pérez-Bravo et al., 2021; Kurihara and Maruyama, 2022). Bentz (2006) suggested that the instantaneous hydration rates of cement particles were linearly related to the volume fractions of water-filling voids and non-hydrated cement (along with fillers), while the final degree of hydration was strongly dependent on the initial water-to-cement ratio. Consequently, the initial water-to-cement ratio to some extent determines the ultimate degree of hydration of the cement pastes.

3.3 Effect of MgO content on the hydration and porosity of LHP paste

The hydration of MgO forms $Mg(OH)_2$, which significantly affects the hydration and pore structure of LHP pastes (Park et al., 2020). Figs. 13–15 illustrate the hydration states of LHP cement pastes with a water-to-cement ratio of 0.40 and different contents of MgO. In these figures, MgO particles with black color are randomly dispersed within the paste. It can be observed that the amount of cyan-colored MH crystals increases with larger MgO content. Since highly reactive MgO is used in this study, as hydration time progresses, MgO tends to react fully, leading to an increased presence of MH crystals in the paste. Figs. 16–18 depict the hydration states of LHP cement pastes with a water-to-cement ratio of 0.45 for different contents of MgO. From a comparison of Figs. 13–18, the primary difference is that an increased water-to-cement ratio results in a diluted paste. Figs. 19–21 depict the hydration states of LHP cement pastes with a water-to-cement ratio of 0.50 and varying contents of MgO. A higher water-to-cement ratio could provide sufficient space for the reaction of MgO, and MgO seems to rapidly react to form many MH crystals. However, the overall compactness of the paste is still primarily determined by the water-to-cement ratio; Figs. 13–21 only reflect the distributions of MgO within the paste at a macroscopic level. Therefore, in this study, the porosities of the paste at different hydration stages are estimated in order to investigate the impact of MgO on the pore structure.

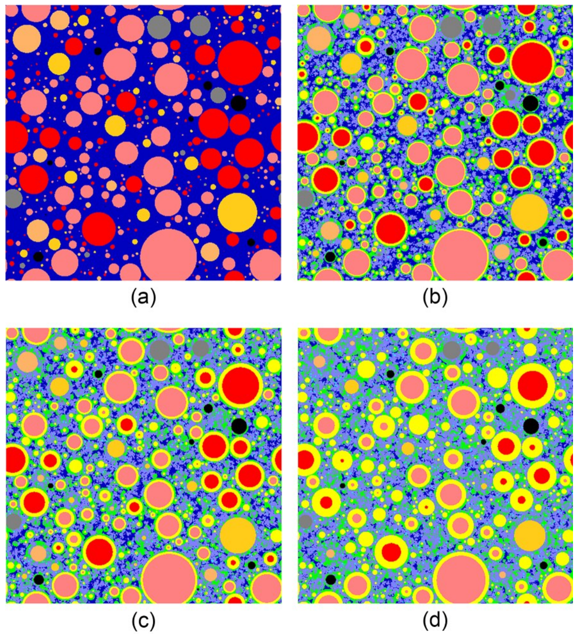

Fig. 13 Cross-sectional diagram of Paste WC04T20M2: (a) initial state; (b) curing for 1 d; (c) curing for 3 d; (d) curing for 27 d

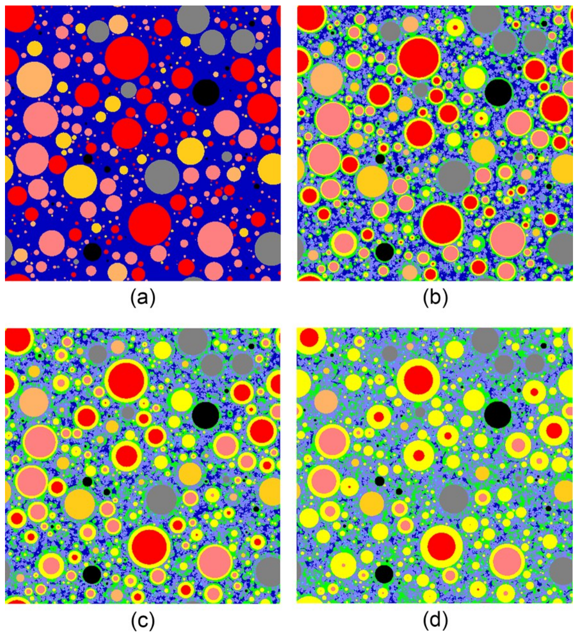

Fig. 14 Cross-sectional diagram of Paste WC04T20M4: (a) initial state; (b) curing for 1 d; (c) curing for 3 d; (d) curing for 27 d

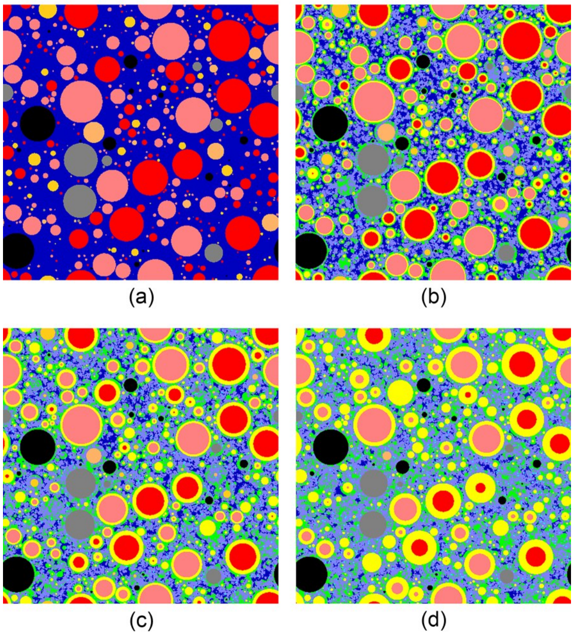

Fig. 15 Cross-sectional diagram of Paste WC04T20M5: (a) initial state; (b) curing for 1 d; (c) curing for 3 d; (d) curing for 27 d

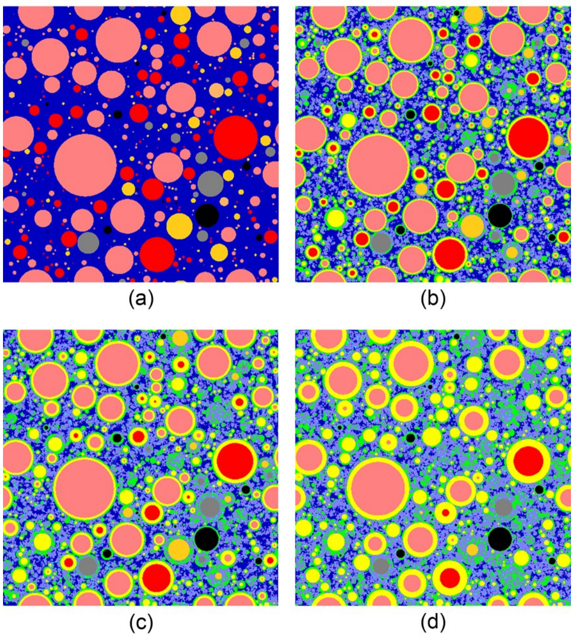

Fig. 16 Cross-sectional diagram of Paste WC045T20M2: (a) initial state; (b) curing for 1 d; (c) curing for 3 d; (d) curing for 27 d

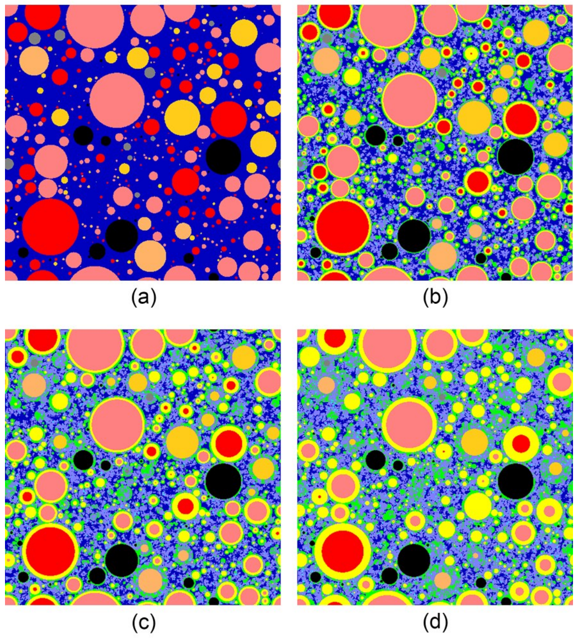

Fig. 17 Cross-sectional diagram of Paste WC045T20M4: (a) initial state; (b) curing for 1 d; (c) curing for 3 d; (d) curing for 27 d

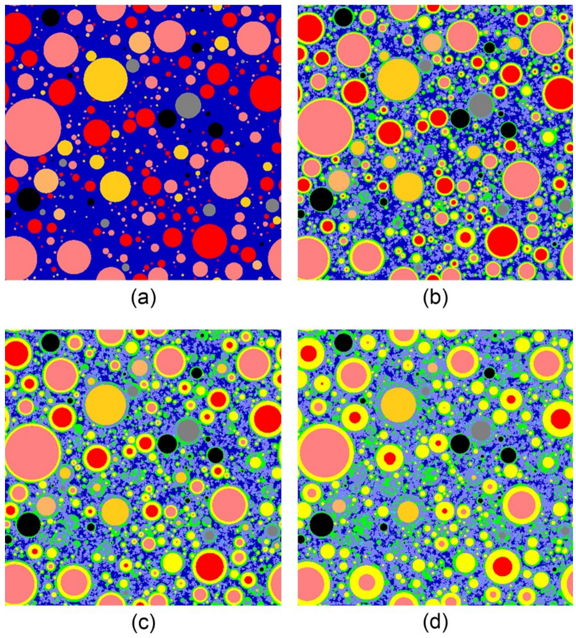

Fig. 18 Cross-sectional diagram of Paste WC045T20M5: (a) initial state; (b) curing for 1 d; (c) curing for 3 d; (d) curing for 27 d

Figs. 22–24 present porosities of LHP pastes with water-to-cement ratios of 0.40, 0.45, and 0.50. As shown in these figures, the trend of porosity with hydration time presents as a typical "L" shape. This indicates that the rapid reduction in porosity occurs primarily during the early stages of paste hydration (Shi et al., 2020). However, it is also evident from Figs. 22–24 that, regardless of MgO content, the differences in

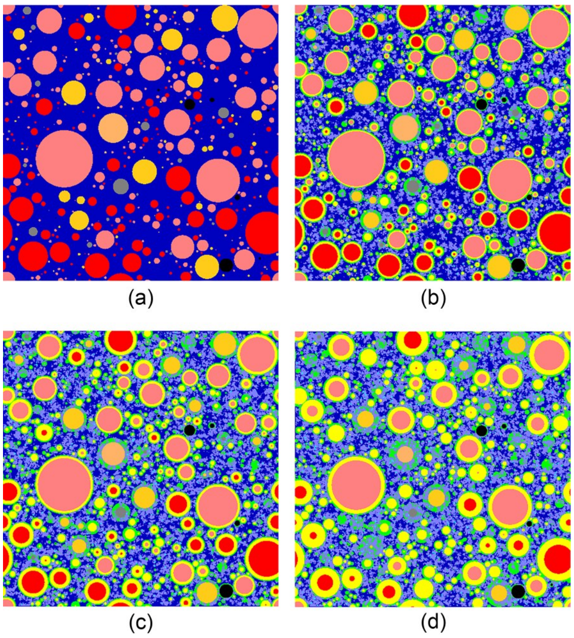

Fig. 19 Cross-sectional diagram of Paste WC05T20M2: (a) initial state; (b) curing for 1 d; (c) curing for 3 d; (d) curing for 27 d

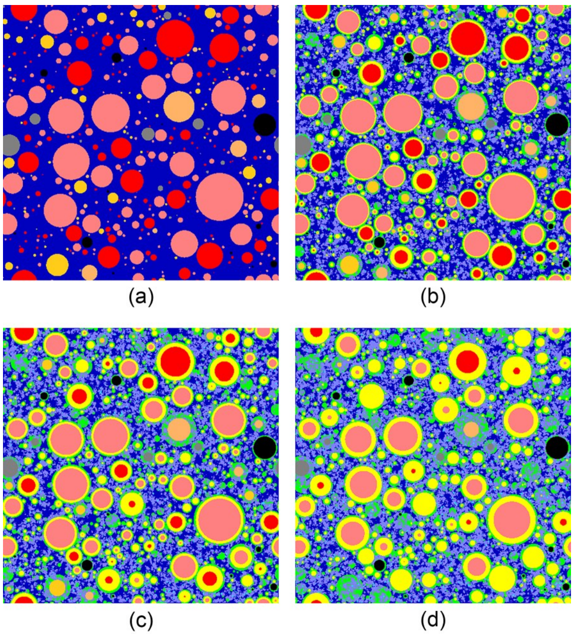

Fig. 20 Cross-sectional diagram of Paste WC05T20M4: (a) initial state; (b) curing for 1 d; (c) curing for 3 d; (d) curing for 27 d

early-stage porosity are smaller compared to those observed at 27 d. This may suggest that the influence of MgO on the porosity of cement paste becomes more pronounced over the long term. For WC04T20M0, the porosity ranges from 17.27% to 5.37% over the

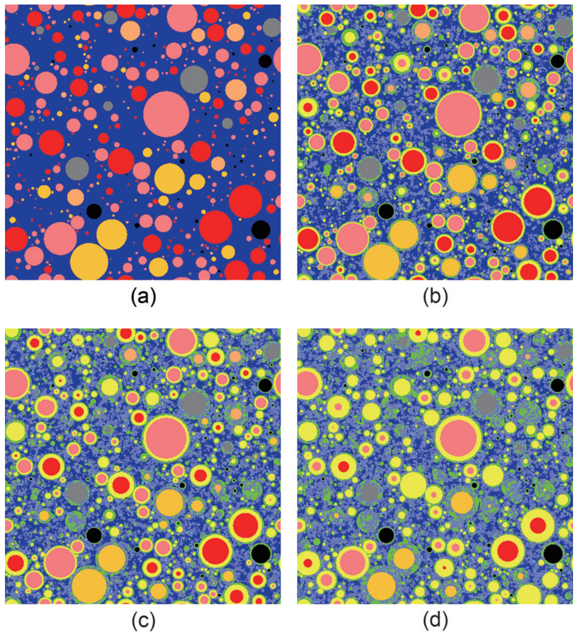

Fig. 21 Cross-sectional diagram of Paste WC05T20M5: (a) initial state; (b) curing for 1 d; (c) curing for 3 d; (d) curing for 27 d

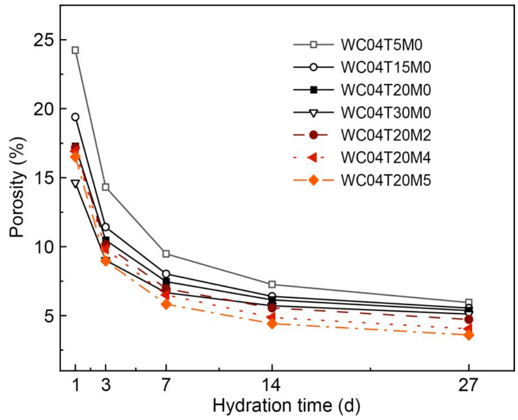

Fig. 22 Porosity of LHP pastes with a water-to-cement ratio of 0.40

hydration time from 1 to 27 d. While the ranges of porosities of WC045T20M0 and WC05T20M0 are from 24.04% to 12.06% and 29.34% to 17.99%, respectively, the porosity decreases by an average of approximately 11.74%. The porosity values obtained from this simulation are similar to those that were obtained using the mercury intrusion porosimetry method for high-belite cement in related studies; the data trend also aligns with the findings of such studies (Shirani et al., 2021).

In Figs. 22–24, it is noteworthy that the addition of MgO enables refinement of the pore structure of

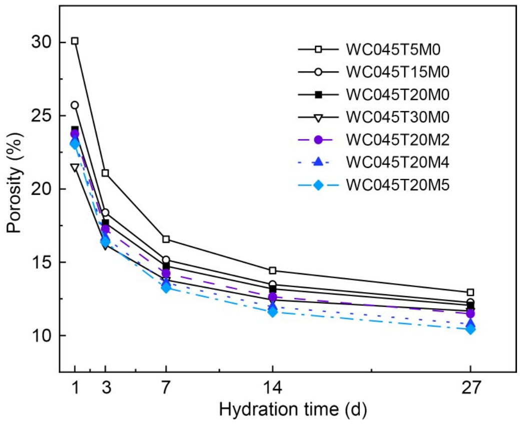

Fig. 23 Porosity of LHP pastes with a water-to-cement ratio of 0.45

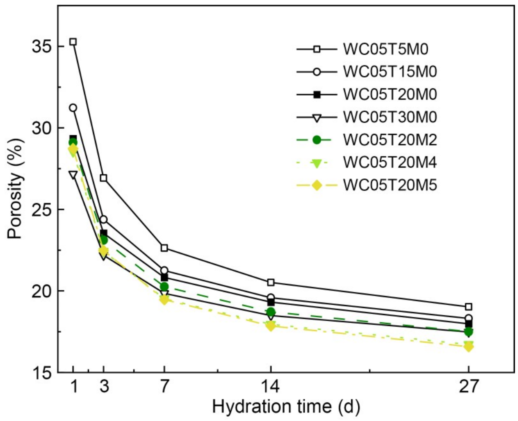

Fig. 24 Porosity of LHP pastes with a water-to-cement ratio of 0.50

all the pastes, due to the expansive effect of MgO. When the water-to-cement ratio is 0.40, a clear trend is observed: as the MgO content increases, its effect on porosity becomes more pronounced. For WC04T20M2, WC04T20M4, and WC04T20M5, the porosity ranges are 17.16%–4.72%, 16.92%–4.04%, and 16.51%–3.59%, respectively. Among these, WC04T20M5 Paste, where the effect of MgO is most significant, shows a porosity decrease of 1.78% compared to WC04T20M0 Paste after 27 d of hydration. This indicates that the addition of MgO can reduce the porosity of the cement paste (Abdel-Gawwad et al., 2018; Nobre et al., 2020). However, for WC045T20M2, WC045T20M4, and WC045T20M5, the porosity ranges are 23.75%–11.49%, 23.30%–10.78%, and 23.04%–10.42%, respectively. For Pastes WC05T20M2, WC05T20M4, and WC05T20M5, the ranges are 29.10%–17.51%, 28.54%–16.72%, and 28.72%–16.58%, respectively. After 27 d of hydration, Pastes WC045T20M5 and WC05T20M5, where the effects of MgO are most significant, show porosity differences of 0.99% and 0.61%, respectively, compared to WC045T20M0 and WC05T20M0.

Especially for pastes with a water-to-cement ratio of 0.50 once the MgO content exceeds a certain level, the effect of MgO on the porosity of the paste becomes limited. The expansive effect of MgO is known to persist over time (Walling and Provis, 2016), and the effect of MgO on the pore structure of cement paste is more pronounced for the case of low water-to-cement ratios. Previous findings have confirmed that due to the high water demand in cement pastes with MgO, when the water content in such pastes is lower, the effect on the pore structure becomes more obvious (Bernard et al., 2023). Xie et al. (2023) conducted a review of the porosity of LHP cement pastes, and pointed out that porosities of LHP cement pastes with a water-to-cement ratio of 0.40 were 33.7% and 24.7% at 3 and 28 d, respectively, with pore size ranging between 3 nm and 1000 μm; this is consistent with the trend of our results presented in Fig. 22. The main discrepancies in the simulated and experimental results lie in the investigated pore ranges.

3.4 Effect of MgO content on the shrinkage of LHP paste

Figs. 25–27 respectively show the autogenous shrinkage values of pastes with water-to-cement ratios of 0.40, 0.45, and 0.50. Expectedly, as the hydration time increases, the autogenous shrinkage values become large, but the rate of increase decreases. After 27 d of hydration, the autogenous shrinkage variation ranges of cement pastes with a water-to-cement ratio of 0.40, 0.45, and 0.50 are 351–367, 339–372, and 331–348 μm/m, respectively. Overall, a large water-cement ratio corresponds to a small autogenous shrinkage of the cement paste. In Section 3.2, it is discussed that a cement paste with a large porosity always has many large capillary pores. According to the Kelvin equation and the Young-Laplace equation, the diameters of these capillary pores are inversely proportional to the capillary pressure (Rijfkogel et al., 2019). Remarkably, for the case of water-cement ratio, the increase in capillary pressure implies a larger value of autogenous shrinkage. This is consistent with the results of Zhou et al. (2014).

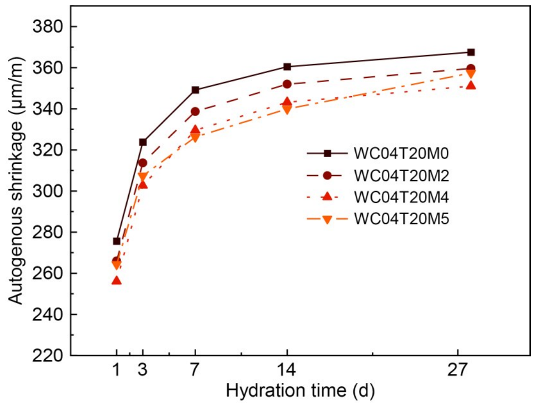

Fig. 25 Autogenous shrinkage value of pastes with a water-to-cement ratio of 0.40

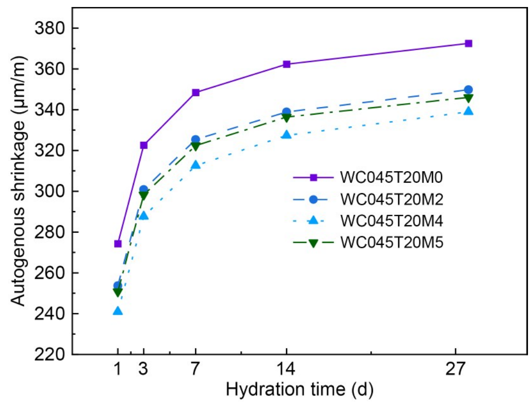

Fig. 26 Autogenous shrinkage value of pastes with a water-to-cement ratio of 0.45

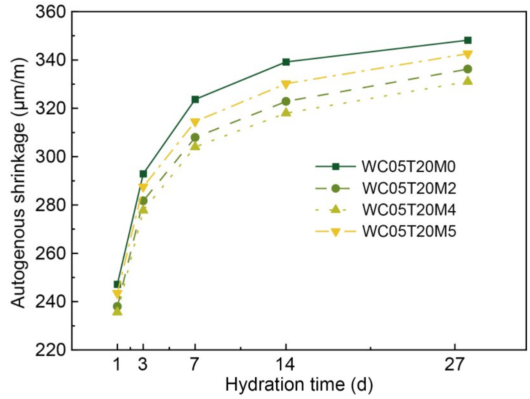

Fig. 27 Autogenous shrinkage value of pastes with a water-to-cement ratio of 0.50

When considering the influence of MgO content, similar trends for cement pastes are observed. In the early stages of hydration, the autogenous shrinkage of cement pastes for varying MgO content is relatively similar. However, as the hydration time increases, the differences in autogenous shrinkage become more obvious. Compared with the blank groups (WC04T20M0, WC045T20M0, and WC05T20M0), the addition of MgO significantly reduces the autogenous shrinkage of pastes at 27 d, due to the expansion caused by the hydration of MgO that generates $Mg(OH)_2$ (Mo et al., 2012). Deng et al. (1990) discovered that such expansion was highly dependent on the location and size of the $Mg(OH)_2$ crystals. During the initial stage, the expansion of the pastes is attributed to the swelling force generated by the water absorption of fine $Mg(OH)_2$ crystals. As the crystals grow, the crystal growth pressure from $Mg(OH)_2$ becomes the dominant expansive force.

Therefore, the expansion generated at an early age is relatively small and can only compensate for a small part of the autogenous shrinkage. As MgO continuously hydrates, the shrinkage of cement paste is gradually compensated for by the expansion generated by the hydration of MgO. Therefore, the differences in shrinkage become more obvious with the increase of age. Compared with autogenous shrinkages of cement pastes with MgO reported in literature (Mo et al., 2010, 2012; 2015, 2019; Zhang, 2022; Chen et al., 2023) and those in this work, even if the dosage and reactivity of the incorporated MgO are similar, there are still great differences in the autogenous shrinkage of pastes at the same age. The reasons for this may be the proportion of cement clinker present, the water-cement ratio, and the utilization of admixtures.

Across the investigated range of MgO content, we find other interesting phenomenon. Under the conditions of this study, the shrinkage compensation effect is the best in cement pastes when the MgO content is 4%, which is consistent with the results of Li et al. (2019). The MgO used in our simulation has high reactivity, and thus, presents a large specific surface area. Such MgO may be prone to agglomeration when its content is high. Apparently, such agglomeration has a negative effect on expansion caused by hydration of MgO. Additionally, previous findings showed that once $Mg(OH)_2$ crystals were quickly generated and wrapped on the surfaces of non-hydrated particles, this was not conducive to the formation of large crystals and led to poor expansion effect (Zhang, 2022). Regardless, our simulation results are in accordance with practical engineering requirements: when the content of MgO is within 5%, the reduction in mechanical properties is very small (Huang et al., 2019).

4 Conclusions

Based on computer simulations, we conducted an in-depth investigation of the hydration process, pore structure, and autogenous shrinkage of LHP cement pastes with different water-to-cement ratios, curing temperatures, and MgO contents. High curing temperature was found to be beneficial for promoting hydration reactions in cement paste. However, in the long-term curing process, the influence of temperature on the hydration process gradually weakens. For the same hydration time and curing temperature, a high water-to-cement ratio results in a larger number of hydrated products in the cement paste. A high water-to-cement ratio corresponds to a large porosity of the paste, which can provide a large space for the cement particles to continue to react. The degree of hydration of cement particles in pastes with high water-to-cement ratios is also relatively high. Moreover, the addition of MgO can reduce the porosity of the paste to a certain extent.

The higher the water-to-cement ratio, the smaller the autogenous shrinkage of the cement paste. With the increase of hydration time, MgO continuously hydrates, and its influence on the autogenous shrinkage continuously grows. When the content of MgO is 4%, the shrinkage compensation effect is found to be the best. This study provides valuable insights for the use of low-heat Portland cement, and future work may extend the analysis to other types of cement.

Acknowledgments

This work is supported by the National Natural Science Foundation of China (Nos. 51602229 and U2040222), the Opening Project of Key Laboratory of Advanced Civil Engineering Materials of Ministry of Education (Tongji University), the Joint Fund Project of Hubei Provincial Natural Science Foundation (No. 2023AFD196), and the Opening Funding of Henan Key Laboratory of Green Building Materials Manufacturing and Intelligent Equipment (No. 2024LGSYS02), China.

Author contributions

Shengwen TANG, Wenwei LI, Yan SHI, and Lei WANG designed the research. Jiajie YIN and Yifan ZHOU processed the corresponding data. Yifan ZHOU and Yang WANG wrote the first draft of the manuscript. Jiajie YIN, Yuxiang PENG, and Yushan WANG helped to organize the manuscript. Yifan ZHOU revised and edited the final version.

Conflict of interest

Wenwei LI, Yifan ZHOU, Jiajie YIN, Yuxiang PENG, Yushan WANG, Shengwen TANG, Yan SHI, Yang WANG, and Lei WANG declare that they have no conflict of interest.

References

Abdel-Gawwad HA, Abo El-Enein SA, Heikal M, et al., 2018. Synergistic effects of curing conditions and magnesium oxide addition on the physico-mechanical properties and firing resistivity of Portland cement mortar. *Construction and Building Materials*, 176:676-689. https://doi.org/10.1016/j.conbuildmat.2018.05.092

Bentz DP, 2006. Influence of water-to-cement ratio on hydration kinetics: simple models based on spatial considerations. *Cement and Concrete Research*, 36(2):238-244. https://doi.org/10.1016/j.cemconres.2005.04.014

Bentz DP, Jensen OM, 2004. Mitigation strategies for autogenous shrinkage cracking. *Cement and Concrete Composites*, 26(6):677-685. https://doi.org/10.1016/S0958-9465(03)00045-3

Bernard E, Nguyen H, Kawashima S, et al., 2023. MgO-based cements–current status and opportunities. *RILEM Technical Letters*, 8:65-78. https://doi.org/10.21809/rilemtechlett.2023.177

Brouwers HJH, de Korte ACJ, 2016. Multi-cycle and multi-scale cellular automata for hydration simulation (of Portland-cement). *Computational Materials Science*, 111:116-124. https://doi.org/10.1016/j.commatsci.2015.08.049

Bullard JW, Jennings HM, Livingston RA, et al., 2011. Mechanisms of cement hydration. *Cement and Concrete Research*, 41(12):1208-1223. https://doi.org/10.1016/j.cemconres.2010.09.011

Chen T, Wang ZH, Bai EL, et al., 2023. Effect of nano admixtures on the engineering properties and microstructure of sulphoaluminate cement mortar at −10 °C. *Construction and Building Materials*, 402:133015. https://doi.org/10.1016/j.conbuildmat.2023.133015

Chen X, Yang HQ, Li WW, 2016. Factors analysis on autogenous volume deformation of MgO concrete and early thermal cracking evaluation. *Construction and Building Materials*, 118:276-285. https://doi.org/10.1016/j.conbuildmat.2016.02.093

Cuesta A, Ayuela A, Aranda MAG, 2021. Belite cements and their activation. *Cement and Concrete Research*, 140: 106319. https://doi.org/10.1016/j.cemconres.2020.106319

Deng M, Cui XH, Liu YZ, et al., 1990. Expansive mechanism of magnesia as an additive of cement. *Journal of Nanjing Institute of Chemical Technology*, 12(4):1-11 (in Chinese).

Fang K, Fall M, 2018. Effects of curing temperature on shear behaviour of cemented paste backfill-rock interface. *International Journal of Rock Mechanics and Mining Sciences*, 112:184-192. https://doi.org/10.1016/j.ijrmms.2018.10.024

Gong JW, Jiang CM, Tang XJ, et al., 2020. Optimization of mixture proportions in ternary low-heat Portland cement-based cementitious systems with mortar blends based on projection pursuit regression. *Construction and Building Materials*, 238:117666.
https://doi.org/10.1016/j.conbuildmat.2019.117666

Hilpert M, Miller CT, 2001. Pore-morphology-based simulation of drainage in totally wetting porous media. *Advances in Water Resources*, 24(3-4):243-255.
https://doi.org/10.1016/S0309-1708(00)00056-7

Huang KJ, Shi XJ, Zollinger D, et al., 2019. Use of MgO expansion agent to compensate concrete shrinkage in jointed reinforced concrete pavement under high-altitude environmental conditions. *Construction and Building Materials*, 202:528-536.
https://doi.org/10.1016/j.conbuildmat.2019.01.041

Jawed I, Goto S, Kondo R, 1976. Hydration of tetracalcium aluminoferrite in presence of lime and sulfates. *Cement and Concrete Research*, 6(4):441-453.
https://doi.org/10.1016/0008-8846(76)90073-9

Karpov IK, Chudnenko KV, Kulik DA, 1997. Modeling chemical mass transfer in geochemical processes; thermodynamic relations, conditions of equilibria and numerical algorithms. *American Journal of Science*, 297(8):767-806.
https://doi.org/10.2475/ajs.297.8.767

Karpov IK, Chudnenko KV, Bychinskii VA, et al., 2001. Minimization of Gibbs free energy in geochemical systems by convex programming. *Geochemistry International*, 39(11): 1108-1119.

Kjellsen KO, Detwiler RJ, 1992. Reaction kinetics of Portland cement mortars hydrated at different temperatures. *Cement and Concrete Research*, 22(1):112-120.
https://doi.org/10.1016/0008-8846(92)90141-H

Kjellsen KO, Detwiler RJ, 1993. Later-age strength prediction by a modified maturity model. *ACI Materials Journal*, 90(3):220-227.

Kotsay G, Jaskulski R, 2019. Belite cement as an ecological alternative to Portland cement—a review. *Materials Structures Technology*, 2(1):70-76.

Kulik DA, Wagner T, Dmytrieva SV, et al., 2013. GEM-Selektor geochemical modeling package: revised algorithm and GEMS3K numerical kernel for coupled simulation codes. *Computational Geosciences*, 17(1):1-24.
https://doi.org/10.1007/s10596-012-9310-6

Kurihara R, Maruyama I, 2022. Revisiting Tennis-Jennings method to quantify low-density/high-density calcium silicate hydrates in Portland cement pastes. *Cement and Concrete Research*, 156:106786.
https://doi.org/10.1016/j.cemconres.2022.106786

Li ZH, Zhang W, Wang RL, et al., 2019. Effects of reactive MgO on the reaction process of geopolymer. *Materials*, 12(3):526.
https://doi.org/10.3390/ma12030526

Lothenbach B, Kulik DA, Matschei T, et al., 2019. Cemdata18: a chemical thermodynamic database for hydrated Portland cements and alkali-activated materials. *Cement and Concrete Research*, 115:472-506.
https://doi.org/10.1016/j.cemconres.2018.04.018

Ma HY, Li ZJ, 2013. Realistic pore structure of Portland cement paste: experimental study and numerical simulation. *Computers and Concrete*, 11(4):317-336.
https://doi.org/10.12989/cac.2013.11.4.317

Mo LW, Deng M, Tang MS, 2010. Effects of calcination condition on expansion property of MgO-type expansive agent used in cement-based materials. *Cement and Concrete Research*, 40(3):437-446.
https://doi.org/10.1016/j.cemconres.2009.09.025

Mo LW, Deng M, Wang A, 2012. Effects of MgO-based expansive additive on compensating the shrinkage of cement paste under non-wet curing conditions. *Cement and Concrete Composites*, 34(3):377-383.
https://doi.org/10.1016/j.cemconcomp.2011.11.018

Mo LW, Deng M, Tang MS, et al., 2014. MgO expansive cement and concrete in China: past, present and future. *Cement and Concrete Research*, 57:1-12.
https://doi.org/10.1016/j.cemconres.2013.12.007

Mo LW, Liu M, Al-Tabbaa A, et al., 2015. Deformation and mechanical properties of the expansive cements produced by inter-grinding cement clinker and MgOs with various reactivities. *Construction and Building Materials*, 80:1-8.
https://doi.org/10.1016/j.conbuildmat.2015.01.066

Mo LW, Fang JW, Hou WH, et al., 2019. Synergetic effects of curing temperature and hydration reactivity of MgO expansive agents on their hydration and expansion behaviours in cement pastes. *Construction and Building Materials*, 207:206-217.
https://doi.org/10.1016/j.conbuildmat.2019.02.150

Nobre J, Ahmed H, Bravo M, et al., 2020. Magnesia (MgO) production and characterization, and its influence on the performance of cementitious materials: a review. *Materials*, 13(21):4752.
https://doi.org/10.3390/ma13214752

Park S, Ma J, Yun TS, et al., 2020. Pore-scale swelling mechanism of magnesium oxide granules during hydration. *Construction and Building Materials*, 251:119101.
https://doi.org/10.1016/j.conbuildmat.2020.119101

Peng HY, Lin P, Xiang YF, et al., 2022. Effects of carbon thin film on low-heat cement hydration, temperature and strength of the Wudongde dam concrete. *Buildings*, 12(6):717.
https://doi.org/10.3390/buildings12060717

Pérez-Bravo R, Morales-Cantero A, Bruscolini M, et al., 2021. Effect of boron and water-to-cement ratio on the performances of laboratory prepared Belite-Ye'elimite-ferrite (BYF) cements. *Materials*, 14(17):4862.
https://doi.org/10.3390/ma14174862

Qian Z, Schlangen E, Ye G, et al., 2010. Predicción de las propiedades mecánicas del cemento en la micro-escala. *Materiales de Construcción*, 60(297):7-18 (in Spanish).

Rijfkogel LS, Ghanbarian B, Hu QH, et al., 2019. Clarifying pore diameter, pore width, and their relationship through pressure measurements: a critical study. *Marine and Petroleum Geology*, 107:142-148.
https://doi.org/10.1016/j.marpetgeo.2019.05.019

Shi JY, Liu BJ, He ZH, et al., 2020. Properties evolution of high-early-strength cement paste and interfacial transition zone during steam curing process. *Construction and*

Building Materials, 252:119095.
https://doi.org/10.1016/j.conbuildmat.2020.119095

Shirani S, Cuesta A, Morales-Cantero A, et al., 2021. Influence of curing temperature on belite cement hydration: a comparative study with Portland cement. *Cement and Concrete Research*, 147:106499.
https://doi.org/10.1016/j.cemconres.2021.106499

Sinyoung S, Kunchariyakun K, Asavapisit S, et al., 2017. Synthesis of belite cement from nano-silica extracted from two rice husk ashes. *Journal of Environmental Management*, 190:53-60.
https://doi.org/10.1016/j.jenvman.2016.12.016

Song SB, Ding QL, Wei JN, 2019. Improved algorithm for estimating pore size distribution from pore space images of porous media. *Physical Review E*, 100(5):053314.
https://doi.org/10.1103/PhysRevE.100.053314

Vahedifard F, Nili M, Meehan CL, 2010. Assessing the effects of supplementary cementitious materials on the performance of low-cement roller compacted concrete pavement. *Construction and Building Materials*, 24(12):2528-2535.
https://doi.org/10.1016/j.conbuildmat.2010.06.003

van Damme H, 2018. Concrete material science: past, present, and future innovations. *Cement and Concrete Research*, 112:5-24.
https://doi.org/10.1016/j.cemconres.2018.05.002

Wagner T, Kulik DA, Hingerl FF, et al., 2012. GEM-Selektor geochemical modeling package: TSolMod library and data interface for multicomponent phase models. *The Canadian Mineralogist*, 50(5):1173-1195.
https://doi.org/10.3749/canmin.50.5.1173

Walling SA, Provis JL, 2016. Magnesia-based cements: a journey of 150 years, and cements for the future? *Chemical Reviews*, 116(7):4170-4204.
https://doi.org/10.1021/acs.chemrev.5b00463

Wang QH, Liu RX, Liu PY, et al., 2022. Effects of silica fume on the abrasion resistance of low-heat Portland cement concrete. *Construction and Building Materials*, 329:127165.

Xie J, Wu ZM, Zhang XH, et al., 2023. Trends and developments in low-heat Portland cement and concrete: a review. *Construction and Building Materials*, 392:131535.

Yang HQ, Wang YC, Zhou SH, 2007. Anti-crack performance of low-heat Portland cement concrete. *Journal of Wuhan University of Technology (Materials Science Edition)*, 22(3): 555-559.

Yang Y, Yao JK, Liu JT, et al., 2024. Evaluation of the thermal and shrinkage stresses in restrained concrete: new method of investigation. *Construction and Building Materials*, 411:134493.
https://doi.org/10.1016/j.conbuildmat.2023.134493

Yi ST, Moon YH, Kim JK, 2005. Long-term strength prediction of concrete with curing temperature. *Cement and Concrete Research*, 35(10):1961-1969.
https://doi.org/10.1016/j.cemconres.2005.06.010

Zhang J, 2022. Recent advance of MgO expansive agent in cement and concrete. *Journal of Building Engineering*, 45:103633.
https://doi.org/10.1016/j.jobe.2021.103633

Zhang MZ, Ye G, van Breugel K, 2010. A numerical-statistical approach to determining the representative elementary volume (REV) of cement paste for measuring diffusivity. *Materiales de Construcción*, 60(300):7-20.
https://doi.org/10.3989/mc.2010.60810

Zhong WL, Fan LF, Zhang YH, 2022a. Experimental research on the dynamic compressive properties of lightweight slag based geopolymer. *Ceramics International*, 48(14): 20426-20437.
https://doi.org/10.1016/j.ceramint.2022.03.328

Zhong WL, Zhang YH, Fan LF, et al., 2022b. Effect of PDMS content on waterproofing and mechanical properties of geopolymer composites. *Ceramics International*, 48(18): 26248-26257.
https://doi.org/10.1016/j.ceramint.2022.05.306

Zhong WL, Zhang YH, Fan LF, 2023a. High-ductile engineered geopolymer composites (EGC) prepared by calcined natural clay. *Journal of Building Engineering*, 63:105456.
https://doi.org/10.1016/j.jobe.2022.105456

Zhong WL, Qiu B, Zhang YH, et al., 2023b. Mesoscopic damage characteristics of hydrophobicity-modified geopolymer composites under freezing-thawing cycles based on CT scanning. *Composite Structures*, 326:117637.
https://doi.org/10.1016/j.compstruct.2023.117637

Zhong WL, Sun YH, Zhao X, et al., 2024. Study on synthesis and water stability of geopolymer pavement base material using waste sludge. *Journal of Cleaner Production*, 445: 141331.
https://doi.org/10.1016/j.jclepro.2024.141331

Zhou SB, Shen AQ, Liang XY, et al., 2014. Effect of water to cement ratio on autogenous shrinkage of pavement cement concrete and its mechanism analysis. *Journal of Highway and Transportation Research and Development*, 8(1):7-12.
https://doi.org/10.3969/j.issn.1002-0268.2013.04.001

Zhou YF, Li WW, Peng YX, et al., 2023. Hydration and fractal analysis on low-heat Portland cement pastes using thermodynamics-based methods. *Fractal and Fractional*, 7(8):606.
https://doi.org/10.3390/fractalfract7080606